We are IntechOpen, the world's leading publisher of Open Access books Built by scientists, for scientists

4,800
Open access books available

122,000
International authors and editors

135M
Downloads

Our authors are among the

154
Countries delivered to

TOP 1%
most cited scientists

12.2%
Contributors from top 500 universities

CLARIVATE ANALYTICS BOOK CITATION INDEX INDEXED

WEB OF SCIENCE™

Selection of our books indexed in the Book Citation Index in Web of Science™ Core Collection (BKCI)

Interested in publishing with us?
Contact book.department@intechopen.com

Numbers displayed above are based on latest data collected.
For more information visit www.intechopen.com

Chapter 8

Structural, Magnetic and Transport Properties of B-Site Substituted Perovskite $La_{0.7}Sr_{0.3}MnO_3$

J.B. Yang, M.S. Kim, T. F. Creel, H. Zhao, X.G. Chen, W.B. Yelon and W.J. James

Additional information is available at the end of the chapter

http://dx.doi.org/10.5772/61770

Abstract

In this chapter, in order to understand the structural related magnetic and transport properties of B site substituted perovskites $La_{0.7}Sr_{0.3}MnO_3$ (LSMO), we have systematically investigated the effects of replacing some of the Mn with nonmagnetic elements Ti, Zr, Cu, Al, Zn and magnetic elements Co, Ni, Cr, Fe. The structural, magnetic and electrical phase transitions and transport properties of these compounds were investigated by neutron diffraction, magnetization and electric resistivity measurements.

The abnormal behaviors relative to the parent manganite perovskite are explained by the competition between the double exchange and super exchange interactions, Mn-O bond distance, Mn-O-Mn bond angle, local Jahn-Teller distortion, the dilution of magnetization, the frustration of spins, and the change of valence states.

Keywords: Pervoskite, crystal structure, magnetic structure, neutron diffraction, magnetic properties

1. Introduction

Perovskite oxides have been an interesting research area for scientists due to their promising physical properties including colossal magnetoresistance (CMR), superconductivity, multiferroelectricity, metal-insulator transition (MIT), charge/orbital ordering, etc. Among various perovskite oxides, the manganite is a representative one with fascinating physical properties [37]. The manganite materials such as $La_{1-x}Sr_xMnO_3$, $Nd_{1-x}Sr_xMnO_3$, and $Pr_{1-x}Ca_xMnO_3$ exhibit rich phase diagram involving spin-charge-orbital ordering, canted antiferromagnetic, antiferromagnetic/ferromagnetic ordering, and electronic phase separation [14, 17, 27, 39]. In addition to the abundant magnetic behavior, the MIT often occurs coincidently with structural or

magnetic transition [17]. Pure $LaMnO_3$ is an A-type antiferromagnetic insulator. La^{3+} can be partially substituted by a divalent cation such as Sr^{2+} or Ca^{2+}, and $La_{1-x}(Sr,Ca)_xMnO_3$ can become a metallic and ferromagnetic material. The Mn ions are in Mn^{3+} and Mn^{4+} states, which both have a local spin (S=3/2) from their t_{2g}^3 orbitals, and Mn^{3+} ion provides an extra electron from the e_g orbital responsible for conduction. The magnetic and electronic properties in these compounds can be explained using Zener's double exchange (DE) interaction [4, 11, 20, 40]. There is ferromagnetic interaction between the spin of the e_g^1 electron in Mn^{3+} and the local spin of t_{2g}^3. By Sr or Ca doping, the holes were introduced into the e_g band near the Fermi energy, which leads to mobile holes and conduction under an electric field. It was revealed that both DE interactions and the strong electron-phonon coupling should be considered to understand the Sr(Ca)-doped systems [10, 19, 30, 31, 35]. Polaron hopping was also proposed as the dominant conduction mechanism below T_C [3, 12, 21, 32, 41].

In the past decades, the A-site doped manganites $A_{1-x}D_xMnO_3$ have been extensively studied with various attractive properties [14, 17, 27, 29, 33, 39]. In contrast, the B-site doped manganites have not been well studied. The substitution for the Mn (B site) has shown dramatic effect on the magnetic and transport properties of the perovskites [1, 2, 5, 6, 36, 38]. Generally, the B-site doping with 3d ions would destroy the ferromagnetic ordering of the Mn network, leading to the changes in the magnetic and electrical properties of manganites. The reentrant spin glass behavior has been observed in the Cr-doped A-type antiferromagnetic $La_{0.46}S_{r0.54}Mn_{1-x}Cr_xO_3$ due to the competing interaction between the FM and the A-type AFM coupling. The charge-orbital ordered $Nd_{0.5}Ca_{0.5}Mn_{1-x}Cr_xO_3$ is a relaxor ferromagnet [26]. The Fe-doped $La_{1-x}Ca_xMnO_3$ has gone through the localization-delocalization transition as the increase of the dopant concentration [1, 34]. Two ferromagnetic phases appeared in the $LaMn_{0.5}Ni_{0.5}O_3$ sample, which is critically related to the preparation process [18].

Therefore, in this chapter, the samples of $La_{0.7}Sr_{0.3}Mn_{1-x}T_xO_3$ (T= Ti, Zr, Cu, Co and Cr) were prepared, and the effects of substitution on Mn were studied using neutron diffraction(ND), X-ray photoelectron spectra (XPS), magnetic and electric resistivity measurements. The relationship between structure and physical properties are explained by the competition between the DE and super exchange interactions, bandwidth W, bond angle, bond length and the frustration of spins and the change of valence states.

2. Experiments

Samples of $La_{0.7}Sr_{0.3}Mn_{1-x}T_xO_3$ (T=Ti, Zr, Cu, Co, Cr) were synthesized using the standard solid-state reaction method, starting with the high purity La_2O_3, MnO_2, TiO_2, CuO, Cr_2O_3, Co_3O_4 and $SrCO_3$ powders. Appropriate amounts of these powders were weighed and mixed according to the desired stoichiometry for each sample, then sintered in air for one day at 800℃, and cooled naturally to room temperature as the raw material. The raw materials were ground and sintered again in air for one day at 1350℃ with a room-air quench. The reacted powders were ground and cold pressed into disks with the thickness of ~2 mm under a pressure of ~10 MPa. These disks were sintered in air for one more day at 1350℃ and cooled naturally to room

http://dx.doi.org/10.5772/61770

temperature. X-ray diffraction of the powders was performed at room temperature using with Cu-Kα radiation. Powder neutron diffraction experiments were performed at the University of Missouri-Columbia Research Reactor (MURR, λ = 1.4875Å) and high resolution powder diffractometer at HZB Germany using neutrons of wavelength (λ = 1.79821Å). The patterns were collected at the temperature range from 5K to 300K. Refinement of the XRD and ND data were carried out using the FULLPROF program. Magnetic measurements were conducted with a SQUID magnetometer (MPMS, Quantum design). The zero-field cooling (ZFC) and field cooling (FC) magnetization curves were measured under applied magnetic field of 50Oe. Magnetoresistance data were collected using a physical properties measurement system (PPMS, Quantum design) with a standard four-point probe method.

3. Results and discussion

3.1. Ti-substituted perovskites, $La_{0.7}Sr_{0.3}Mn_{1-x}Ti_xO_3$ [22]

Ti-substituted perovskites $La_{0.7}Sr_{0.3}Mn_{1-x}Ti_xO_3$, with $0 \le x \le 0.20$ were studied using XRD, ND, magnetizatic and magnetoresistance (MR) measurements [22]. Typical ND patterns of the $La_{0.7}Sr_{0.3}Mn_{1-x}Ti_xO_3$ (x=0.05, 0.1 and 0.2) were shown in Fig. 1. All samples show a rhombohedral structure (space group $R\bar{3}c$) from RT to 10 K. The crystal structure of the samples can be well fitted with the rhombohedral space group (No. 167), and the atomic positions of La(Sr): 6a (0,0,1/4), Mn(Ti): 6b (0,0,0); O18e (x,0,1/4). The magnetic structure was refined with P1 space group. It was confirmed that the Ti ions replaced the Mn ions at B sites, since the ionic radius of Ti^{4+} (0.605Å) lies between the ionic radius of Mn^{4+} (0.530 Å) and Mn^{3+} (0.645 Å)[38]. Fig. 2 plots the lattice parameter of the samples at different temperatures. It can be seen that the different behaviours are observed at RT and 10K. The lattice parameter *a* and unit cell volume reach a maximum value for x = 0.10, and then decrease for x > 0.10, while lattice parameter *c* increases with increasing x at 10 K. However, at RT, the lattice parameters *a*, *c* and the unit cell volume *V* all show similar increasing trend with increasing Ti content x. This difference should be related to the different magnetic ordering temperatures due to Ti substitution. In this system, as Mn ions are substituted by Ti ions, a lattice distortion may occur. We have calculated the so-called tolerance factor *t* of the $La_{0.7}Sr_{0.3}Mn_{1-x}Ti_xO_3$, which can be used to indicate the geometric measure of size mismatch of perovskites. The calculated values of *t* are about 0.928 and 0.921 for $La_{0.7}Sr_{0.3}MnO_3$ and $La_{0.7}Sr_{0.3}Mn_{0.8}Ti_{0.2}O_3$, respectively. These values are in the stable range of the $0.89 < t < 1.02$ for the rhombohedral structure. The decrease of the *t* will lead to the decrease of Mn-O-Mn bond angle from 166.5 º to 165 º for x=0 and x=0.2 without a structure change.

Fig. 3 plots the average Mn-O bond length and Mn-O-Mn bond angle of $La_{0.7}Sr_{0.3}Mn_{1-x}Ti_xO_3$ obtained from the ND refinement at 10 K and RT. At 10 K, the Mn-O bond length increases up to $x = 0.10$ and keeps constant for $x>0.10$, while the Mn-O-Mn bond angle decreases with increasing x. At RT, the bond length of Mn-O increases up to x = 0.15 and keeps constant for $x \ge 0.15$, while the Mn-O-Mn bond angle decreases and reaches a minimum value for x = 0.15. The changes in the bond length and bond angle of MnO_6 octahedral may help to diminish the internal strain induced by Ti substitution. The Ti substitution will change the oxygen positions

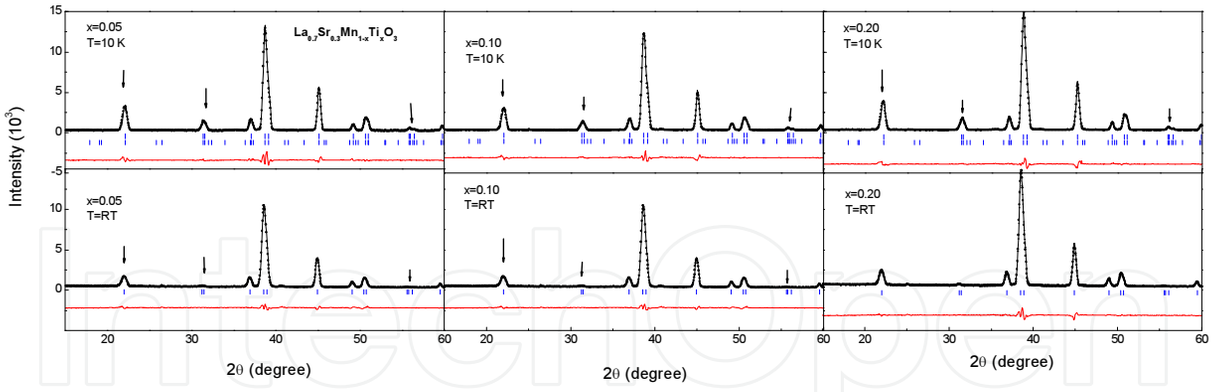

Figure 1. ND patterns of $La_{0.7}Sr_{0.3}Mn_{1-x}Ti_xO_3$ (x = 0.05, 0.10, 0.20) at RT and 10 K. (The bottom curves (red line) are the difference between experimental data and the refinement data. The vertical bars (blue line) represent the magnetic (bottom) and Bragg (top) peak positions). Arrows shows some of the major magnetic diffraction peaks.

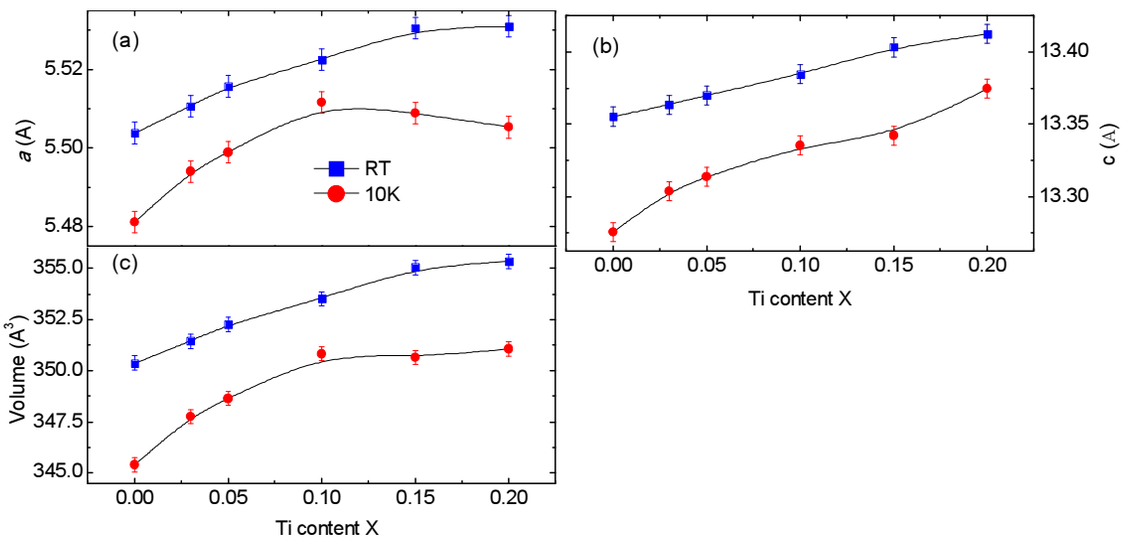

Figure 2. Lattice parameters a, c, and unit cell volumes of $La_{0.7}Sr_{0.3}Mn_{1-x}Ti_xO_3$ with different Ti content x at 10 K and RT.

and affect the Mn-O bond length and the Mn-O–Mn bond angle. This is consistent with the change of the tolerance factor, indicating the increase of Mn-O bond length and the decrease of Mn-O-Mn bond angle are related.

The temperature dependent resistivities for $La_{0.7}Sr_{0.3}Mn_{1-x}Ti_xO_3$ compounds (x = 0.0(a), 0.05(b), 0.10(c), and 0.15(d)) under magnetic fields H = 0, 1, 3, and 5 T were plotted in Fig. 4.

As a comparison, the Curie temperatures *Tc* of the samples are also shown in the figure 4. It can be seen that the resistivity for the $x \leq 0.05$ sample shows a metallic-like behavior below the T_C. A MIT is observed for all the $x \geq 0.10$ samples at low temperature. A maximum peak in the resistivity is observed below T_C for all samples, and shifts to a lower temperature when x increases. The one-electron bandwidth *W* is one of the fundamental parameters for controlling

http://dx.doi.org/10.5772/61770

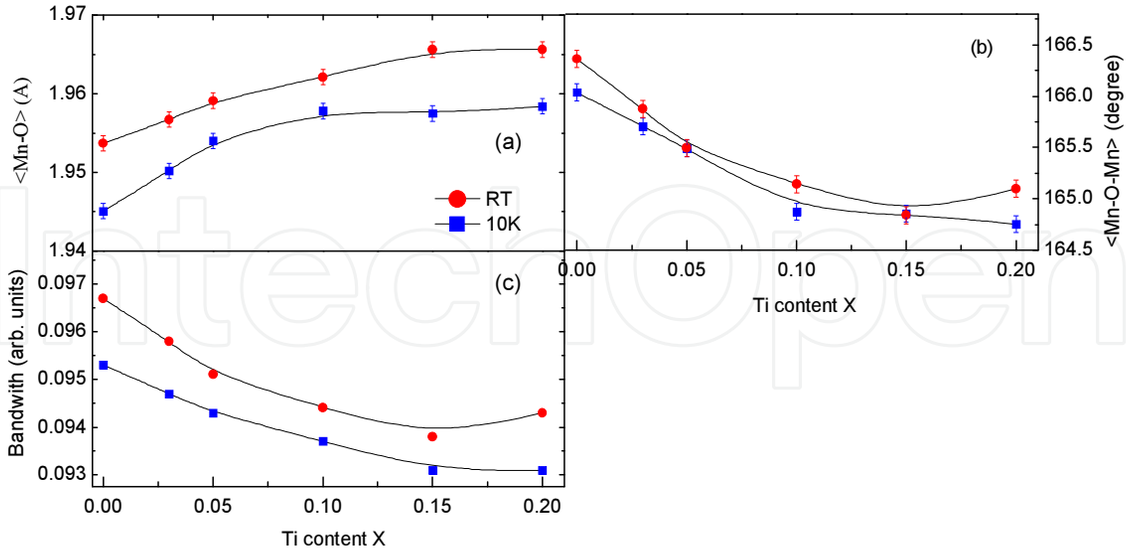

Figure 3. Average Mn-O bond lengths (a), Mn-O-Mn bond angles (b), and electronic bandwidth parameter *W* (c), of $La_{0.7}Sr_{0.3}Mn_{1-x}Ti_xO_3$ at room temperature and at 10K.

the magnetic and electric behavior of correlated electrons system such as perovskite [15, 35]. Using the tight binding approximation, the empirical formula of the *W* for ABO_3-type perovskites is [29].

$$W = \frac{\cos\beta}{(d_{Mn-O})^{3.5}} \tag{1}$$

where $\beta = (\pi - \theta_{<Mn-O-Mn>})/2$, d_{Mn-O} is the average Mn-O bond length, and $\theta_{<Mn-O-Mn>}$ is the average Mn-O-Mn bond angle. By using the data obtained from ND refinements, the calculated values of the *W* are plot in Fig. 3 (c). It is obvious that *W* decreases with the increasing Ti content x, which will reduce the 2p-3d hybridization between O and Mn ions and increases the electron-phonon coupling. Therefore, it leads to a lower magnetic ordering temperature T_C and higher resistivity with increasing Ti content. Since the double exchange interaction between Mn-Mn ions is strongly dependent on both bond angle and bond distance, the substitution of Mn by Ti will decrease the exchange interaction between Mn-Mn ions.

It is obvious that a field-induced shift of the resistivity maximum occurs for x> 0.05 samples. The MR ratio increases with the Ti content x, and reaches to about 70% for $La_{0.7}Sr_{0.3}Mn_{0.8}Ti_{0.2}O_3$, which is related to the weaker magnetic interaction between Mn-Mn ions. The separation of T_C and the resistivity maximum temperature $T_{\rho,max}$ becomes wider as Ti content increases due to the weak coupling between the magnetic ordering and the resistivity as compared with $La_{0.7}Sr_{0.3}MnO_3$.

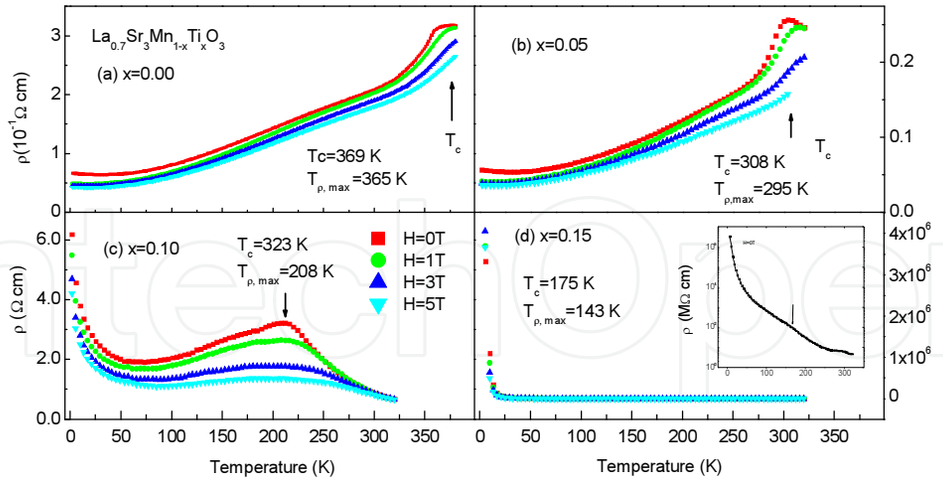

Figure 4. The temperature dependent resistivity for $La_{0.7}Sr_{0.3}Mn_{1-x}TixO_3$ compounds (x = 0.0(a), 0.05(b), 0.10(c), and 0.15(d)) under magnetic field H = 0, 1, 3, and 5T. Arrows indicate the resistivity maximum temperature $T_{\rho,max}$. The inset in (d) is the plot of resistivity of x = 0.15 compound (with log scale) in H = 0T.

3.2. Zr-substituted perovskites $La_{0.7}Sr_{0.3}Mn_{1-x}Zr_xO_3$[23]

We have tried to synthesize the $La_{0.7}Sr_{0.3}Mn_{1-x}Zr_xO_3$ compounds with different Zr contents. However, it was found that solubility limit of Zr is about x ~ 0.10, due to the large size (0.72 Å) of Zr^{4+}. Fig. 5 is the ND patterns of $La_{0.7}Sr_{0.3}Mn_{1-x}Zr_xO_3$. It reveals that Zr goes only to the Mn-site. A single phase of $La_{0.7}Sr_{0.3}Mn_{1-x}Zr_xO_3$ was obtained for x≤0.1, which exhibits a rhombohedral structure from 10 K to RT. An impurity $La_2Zr_2O_7$ phase was found for x>0.1 samples. The refined lattice parameters *a*, *c* and unit cell volume increase with Zr content due to the large ionic radius of the Zr ions as compared to that of the Mn ions.

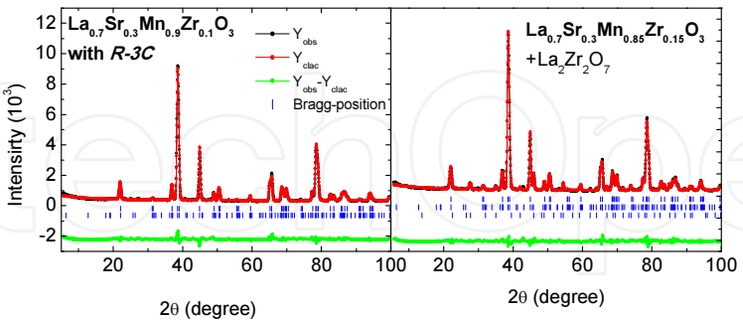

Figure 5. Neutron diffraction patterns of $La_{0.7}Sr_{0.3}Mn_{0.9}Zr_{0.1}O_3$ and $La_{0.7}Sr_{0.3}Mn_{0.85}Zr_{0.15}O_3$ at room temperature.

Fig. 6 plots the average Mn-O bond length,Mn-O-Mn bond angle and bandwidth W obtained from the refined ND patterns at RT and 10K. Similar to those of the Ti substituted samples, the Mn-O bond length increases, while Mn-O-Mn bond angle and band width W decrease with the increase of Zr content. The decrease of the bandwidth W will reduce the overlap between the O-2p and the Mn-3d orbitals, which will reduce the exchange interactions between Mn-

http://dx.doi.org/10.5772/61770

Mn in this system. This is confirmed by the results that the reduction in magnetic moments and the Curie temperature with increased Zr content. A metallic-like behavior was observed for the $La_{0.7}Sr_{0.3}Mn_{1-x}Zr_xO_3$ at low temperature. The contribution from the two-magnon scattering in resistivity becomes larger with increasing Zr content.

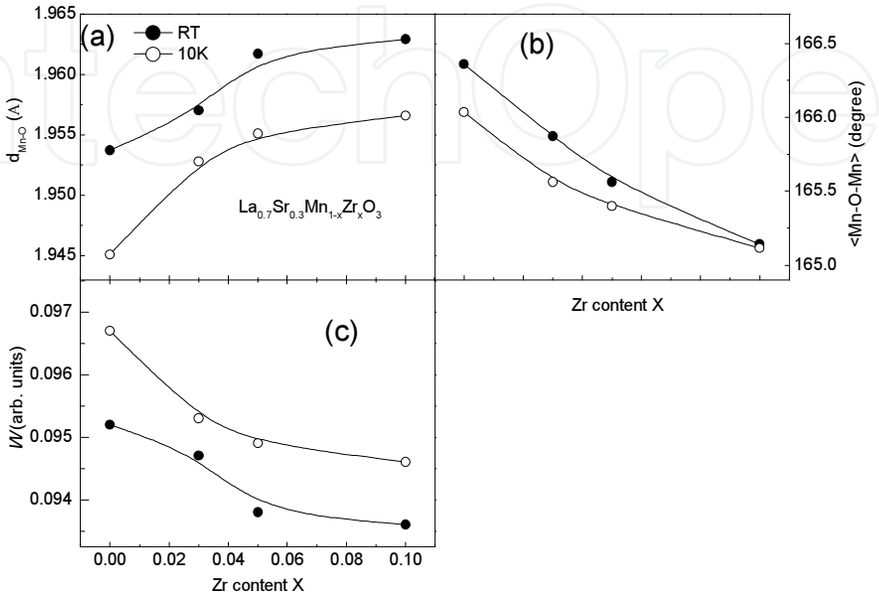

Figure 6. Average Mn-O bond lengths (a), Mn-O-Mn bond angles (b), and electronic bandwidth parameter *W*, of $La_{0.7}Sr_{0.3}Mn_{1-x}Zr_xO_3$ (x = 0.0, 0.03, 0.05, 0.10) at room temperature and at 10K.

3.3. Cu-substituted perovskites $La_{0.7}Sr_{0.3}Mn_{1-x}Cu_xO_3$ [24, 25]

$La_{0.7}Sr_{0.3}Mn_{1-x}Cu_xO_3$ samples with 0 n_p x $z_{i\alpha}$ 0.20 were prepared. XRD and ND patterns indicate that Cu goes into the Mn sites and all samples can be refined with the rhombohedral structure with the R $\bar{3}$ c space-group from 10 K to RT [24, 25]. It was noticed that the lattice parameters a,c and the unit cell volumes decrease with increasing Cu content at RT, while they remain nearly constant with increasing Cu content at 10 K. Since Cu^{2+} has a larger radius (0.73Å) than those of Mn^{3+} and Mn^{4+}, both Cu^{2+} and Cu^{3+} states may appear in these compounds accounting for the abnormal changes of the unit cell volume and the lattice parameters with Cu content. The refined magnetic moments of Mn atoms at 10 K and RT decrease with increasing Cu content. These results agree well with the values obtained from magnetic measurements. There is no sign of antiferromagnetic couplings between Cu and Mn ions.

Fig. 7 plots the Mn-O bond length and Mn-O-Mn bond angle obtained from the ND data. The changes of the Mn-O bond length vs. Cu content show similar trend corresponding to the changes of lattice parameters at 10 K and RT. The average bond angle increases and reaches to a maximum at x = 0.10, then slightly decreases for x > 0.1 at 10K an RT. The bandwidth *W* of the Cu substituted samples shows different effects as compared those of Ti and Zr substituted samples. At 10 K, an increase of the bandwidth *W* with Cu content *x* was observed, which may be related to the Cu valence states(See later discussion). This will affect the exchange

mechanisms and magnetic interactions in this system and is observed through the reduction in ferromagnetic moments with increased Cu content. This indicates a likely reduction in the Mn^{3+}-O-Mn^{4+} ferromagnetic double exchange interactions, a direct result of the reduction in Mn^{3+} ions.

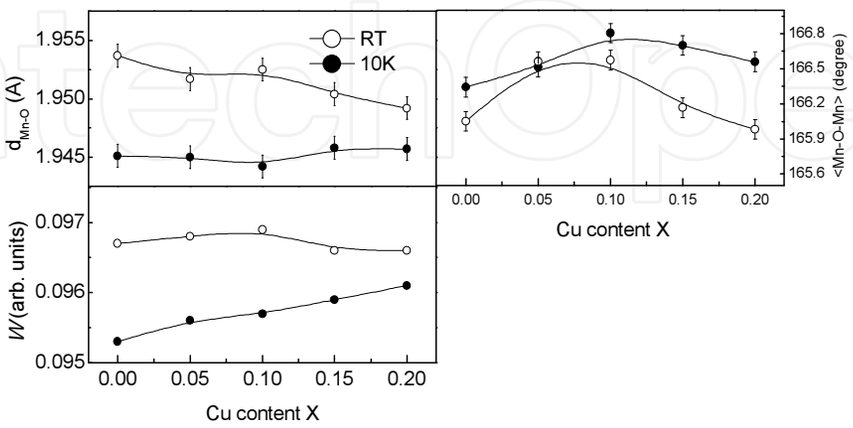

Figure 7. The average Mn-O bond lengths (a), Mn-O-Mn bond angles (b) and band width (c) of $La_{0.7}Sr_{0.3}Mn_{1-x}Cu_xO_3$ at RT and at 10 K.

X-ray photoelectron spectra (XPS) was used to determine the Cu valence states in these compounds. Fig. 8 plots the mole percent of different Cu ions in the Mn sites obtained by fitting the XPS data. The Two kinds of Cu ions (Cu^{3+} and Cu^{2+}) were observed when x > 0.1, unlike the other metal substituted systems. The binding energies of both Cu^{2+} and Cu^{3+} states shift to the lower BE energy region, which suggests a strong hybridization between the Cu-*2p* state and the O-*1s* state.

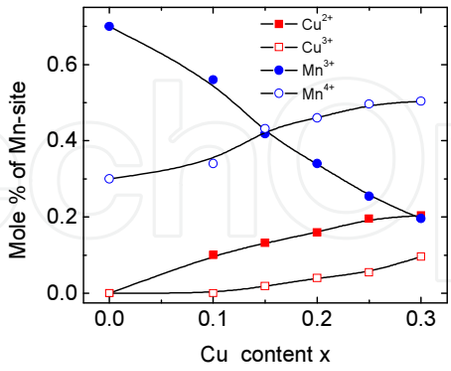

Figure 8. The mole percent of different Cu ions in the Mn sites obtained from XPS

Fig. 9 plots the Curie temperatures for the Cu substituted samples. The T_C decreases with increased Cu content. It was found that the low Cu-doped samples (x= 0.05, Tc=365 K) show almost no decrease in T_C as compared to the parent LSMO. This suggests that the Cu-doping could enhance the exchange coupling of Mn^{3+}-Mn^{4+} due to the Cu^{2+}, and increase the magnetic

http://dx.doi.org/10.5772/61770

ordering temperature T_C at a low Cu-doping ratio. At a high doping ratio, the magnetic dilution effect of Cu is predominant, which gives rise to a sharp drop in the Curie temperature (Tc=250 K) for x=0.15. This is also related to the Cu ionic states. While the signature separation between the zero field cooling(ZFC) and field cooling (FC) curves is present, the complex curves observed in the other 3d-substituted systems is only weakly observable in the x=0.15 sample. This indicates there may be antiferromagnetic ordering up to 50 K that is too small to be observable within the resolution of the neutron diffraction analysis.

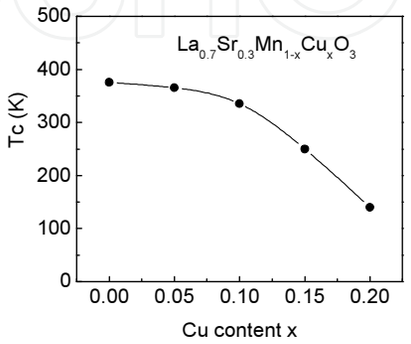

Figure 9. The Curie temperature of $La_{0.7}Sr_{0.3}Mn_{1-x}Cu_xO_3$.

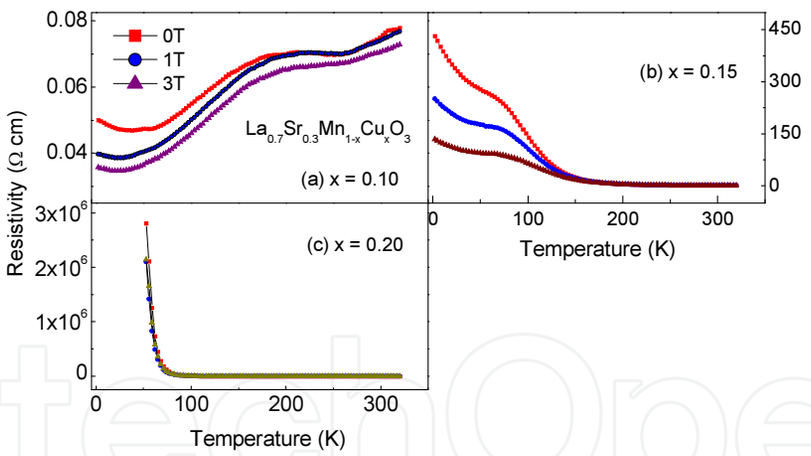

Figure 10. Temperature dependent resistivities of $La_{0.7}Sr_{0.3}Mn_{1-x}Cu_xO_3$ (x = 0.10(a), 0.15(b), 0.20(c)) under applied magnetic fields of H = 0, 1, and 3T.

The temperature dependence of resistivity under various applied fields was measured using PPMS and shown in Fig. 10. With increasing Cu content, the resistivity of the compound increases, while the resistivity decreases with increasing magnetic field. This is ascribed to a reduction of the Mn^{3+}/Mn^{4+} ratio to account for the DE interaction and a reduction in the number of hopping electrons and hopping sites by Cu substitution. The resistivity shows a metal-like behavior with decreasing temperature when x is less than 0.10 samples. A MIT occurs for the $x \geq 0.15$ samples (Fig. 10). A resistivity peak corresponding to the magnetic transition is present.

The suppression of the resistivity by the applied magnetic field occurs over the entire temperature range for all samples. The highest MR ratio of about 80% was obtained for x = 0.15 sample, which might result from the co-existence of Cu^{3+}/ Cu^{2+} and the dilution effect of Cu-doping on the double exchange interaction [25].

3.4. Co-substituted $La_{0.7}Sr_{0.3}Mn_{1-x}Co_xO_3$

Typical ND patterns for the $La_{0.7}Sr_{0.3}Mn_{1-x}Co_xO_3$ samples at RT are shown in Figure 11. It is obvious that the peak intensity of (012) decreases and those of (110) and (104) increase with the increase of the cobalt content x, which is due to the different scattering lengths of Mn and Co ions. Since these peaks are related to magnetic scattering, the changes correspond to the decrease of the magnetic contribution. A Rietveld refinement for all the polycrystalline samples was carried out to understand the detailed crystal and magnetic properties. Figure 12 displays the refined lattice parameters for the $La_{0.7}Sr_{0.3}Mn_{1-x}Co_xO_3$ samples at RT. It shows that the lattice parameters and unit cell volume decrease with increasing the Co content due to the fact that the radius of Co ions (0.55 Å for Co^{3+} and 0.40 Å for Co^{4+}) is smaller than that of Mn ions (0.65 Å for Mn^{3+} and 0.53 Å for Mn^{4+}). Generally speaking, the DE interaction strength among Mn^{3+} and Mn^{4+} can be estimated using the transfer integral, $t \propto \cos(\theta/2)$ and thus strongly depends on the Mn-O-Mn bond angle. The changes in θ value also have strong influence on the effective bandwidth *W*. For a charge-transfer insulator, the band gap energy *Eg* in the insulating phase can be written as $E_g = \Delta - W$, where Δ is the charge-transfer energy and W is the O-2p-like bandwidth (Kim et al., 2005). In fact, Δ changes little in the $La_{1-x}Sr_xMnO_3$ system thus the bandwidth *W* becomes a main factor in turning the band gap energy [16]. The decrease of bandwidth for Co-substituted compounds reduces the overlap between the O-2p and the Mn-3d orbitals. It also increases the band gap energy *Eg*, which in turn decreases the fragile double exchange coupling of Mn^{3+}-O-Mn^{4+}, as well as the magnetization and Curie temperature Tc (375 K for $La_{0.7}Sr_{0.3}MnO_3$, 226 K for $La_{0.7}Sr_{0.3}CoO_3$, and 184, 193, 180 K for x=0.4, 0.5 and 0.6, respectively), with the transition from the metal to insulator.

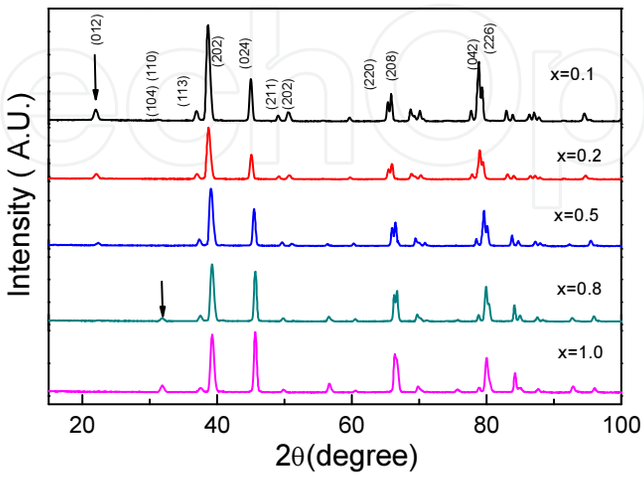

Figure 11. Neutron diffraction patterns of the $La_{0.7}Sr_{0.3}Mn_{1-x}Co_xO_3$ sample at RT.

http://dx.doi.org/10.5772/61770

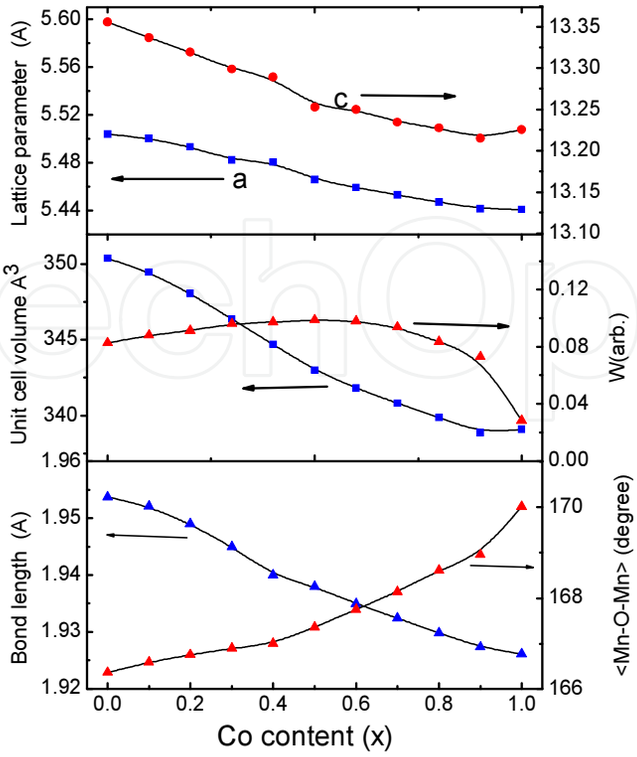

Figure 12. The lattice parameters a, c, unit cell volume, bandwidth *W*, bond length $d_{Mn\text{-}O}$, and bond angle <Mn-O-Mn> for $La_{0.7}Sr_{0.3}Mn_{1-x}Co_xO_3$ at RT.

The temperature dependent ND patterns of $La_{0.7}Sr_{0.3}Mn_{1-x}Co_xO_3$ (x=0.4, 1.0) samples are shown in Figure 13(a). The representative Bragg reflections of neutron diffraction prior to and with the addition of magnetic phase are shown in Figure 13(b). The misfits indicate the magnetic contributions. It is obvious that the (012) reflection has both nuclear and magnetic intensities and the (104), (110) reflections show little magnetic intensity for x=0.4. However, for x=1.0 sample, the (012) peak has magnetic intensity only and (104), (110) has both nuclear and magnetic intensities. There is almost no change of the intensity for x=0.5 and x=0.6 samples whether to add magnetic phase or not. The intensity of the magnetic peak (012) for LSCO decreases with the increase of temperature until vanishes finally, which is similar to LSMO-Co0.4 (i.e. the magnetic peaks (104), (110)).

The Curie temperature (T_C), the coercivity ($_iH_C$), the magnetization and the resistivity of $La_{0.7}Sr_{0.3}Mn_{1-x}Co_xO_3$ are shown in Figure 1. The critical Co-doping contents for the onset/disappearance of the glassy behavior are x=0.3 and 0.8. The $_iH_C$ and resistivity show a maximum value, while the T_C and magnetization show a minimum value at the critical Co-doping point (x=0.3, 0.8). The ferromagnetic ordered $La_{0.7}Sr_{0.3}MnO_3$ gradually turns into disordered glassy system by the B site Co-doping, which is attributed to the break of the double exchange interaction between Mn-Mn ions and random substitution of the Mn ions. At the intermediate Co-doping region, the ferromagnetic ordered clusters embed in the antiferromagnetic ordering cluster matrix, forming the superparamagnetic-like free spin and reentrant spin glassy states. The resistivity increases due to the break of the double exchange interaction and the phase

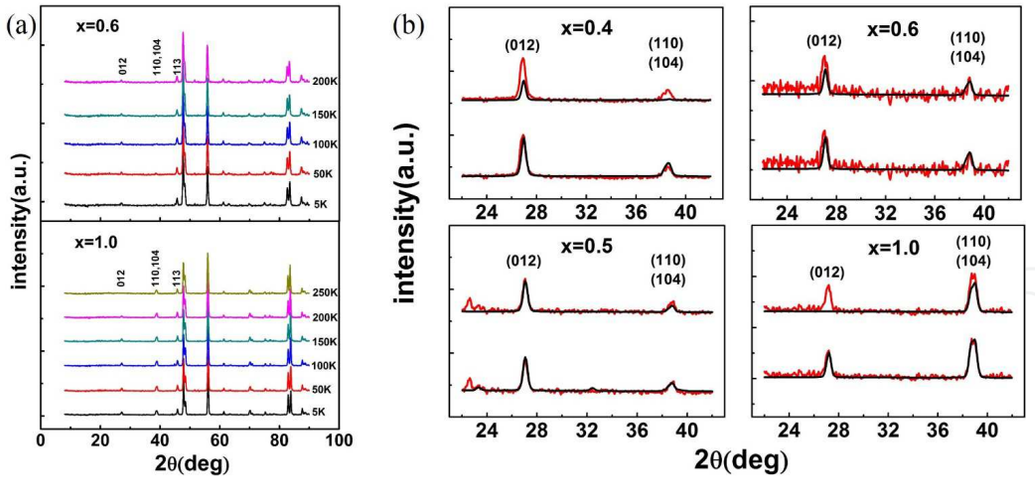

Figure 13. (a) ND patterns for the $La_{0.7}Sr_{0.3}Mn_{1-x}Co_xO_3$ (x=0.4, 1.0) samples at different temperature. (b) Representative Bragg reflections of neutron diffraction data for the $La_{0.7}Sr_{0.3}Mn_{1-x}Co_xO_3$ (x=0.4, 0.5, 0.6, 1.0) samples. Each data graphic contains two groups of plot (red for the experimental data and black for the refined data), the under one with the nuclear and magnetic phase refined and the upper one with only the nuclear phase.

separation. And the destruction of the long range exchange coupling leads to the decrease of the Curie temperature. The sparsely alignment of the cluster makes the decrease of the magnetization

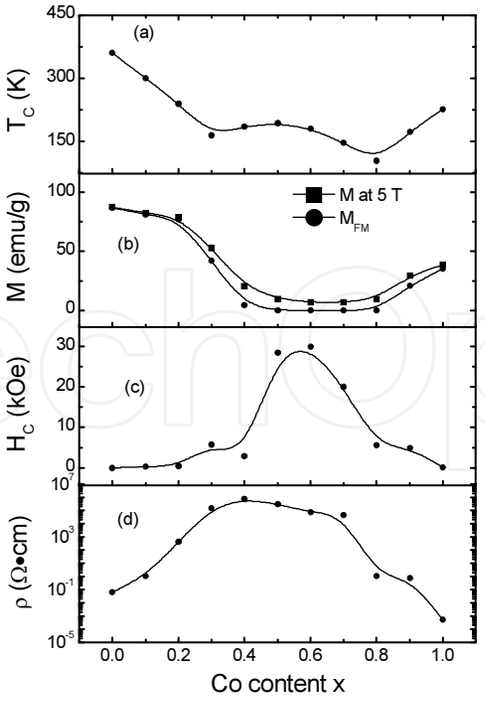

Figure 14. (a) Curie temperature (TC), (b) the magnetization at the field of 5 T and the ferromagnetic component extracted from the M-H curve, (c)the coercivity at 5 K, (d) the resistivity at 70 K of $La_{0.7}Sr_{0.3}Mn_{1-x}Co_xO_3$.

http://dx.doi.org/10.5772/61770

The typical hysteresis loops at various temperatures for $La_{0.7}Sr_{0.3}Mn_{0.5}Co_{0.5}O_3$ were plotted in figure 15. This is a representative one for the intermediate Co-doping samples (0.2<x<0.8), which is consistent with the simple cluster model (where the Co^{3+}-Co^{4+} or Mn^{3+}-Mn^{4+} ferromagnetic clusters exist in the Co^{3}+-Co^{3}+(Mn^{3+}) or Co^{4+}-Co^{4+}(Mn^{4+}) antiferromagnetic cluster). It should be noted that the hysteresis loop at 5K shows a jump at the vicinity of 0 T. The jump disappears when the temperature is just above the Curie temperature. This suggests that the observed phenomenon is related to the competition between the ferromagnetic double exchange interaction and the antiferromagnetic superexchange interaction. The $_iH_{C\ i}$s are significantly enhanced due to the freezing and pinning of the domain wall. The hysteresis loops do not show saturation under a magnetic field of 5T, which is consistent with the cluster glass behaviour. It is proposed that under a high magnetic field, the ferromagnetic clusters and partial antiferromagnetic clusters are forced to align along the direction of magnetic field. But the magnetization could not be saturated on account of the existence of antiferromagnetic clusters, so partial soft ferromagnetic clusters with small coercivity are demagnetized easily around H=0. As a result, a sudden drop of the magnetization has occurred, giving rise to a jump in the hysteresis curve.

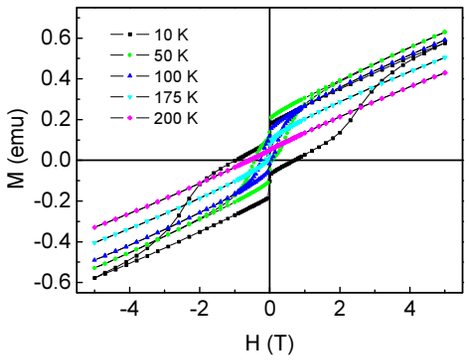

Figure 15. The hysteresis loops of $La_{0.7}Sr_{0.3}Mn_{0.5}Co_{0.5}O_3$ at different temperatures.

3.5. Cr-doped $La_{0.7}Sr_{0.3}Mn_{1-x}Cr_xO_3$ [7, 8, 9]

The $La_{0.7}Sr_{0.3}Mn_{1-x}Cr_xO_3$ (0<x<0.6) have been prepared and influence of the Cr^{3+} substitution for Mn^{3+} was investigated [7, 8, 9]. Figure 14 is the ND patterns of $La_{0.7}Sr_{0.3}Mn_{1-x}Cr_xO_3$ (0<x<0.5) at 10 K. The magnetic contributions to the (012) and (110)+(104) peaks are evident. For x<0.2, the samples are simple ferromagnetic with magnetic moments decreasing with increasing Cr content. For 0.2≤x≤0.4, the (104) + (110) reflections become weaker, but two new peaks ((003) + (011)), inconsistent with a simple ferromagnetic solution emerge. The ((003) + (011)) peak is purely magnetic, while the (113) peak has nuclear and magnetic components. For x=0.5, the (104) + (110) reflections are present but weak, while the (003) + (011) reflections are now dominant. A single, homogeneous, long-range magnetically ordered state with compositionally-dependent charge ordering was proposed to fit the ND patterns [8, 9]. The magnetic structures are related to the competition between Mn-Mn, Mn-Cr and Cr-Cr interactions (double-exchange and superexchange). The metal to semi-metal and semi-metal to insulator

transitions can be quantitatively described as due to the localization effect of superexchange. The presence of charge ordered states above the M-I transition concentration (x) arises from the favourable energetics of Mn^{4+}-O-Cr^{3}+ superexchange bonds relative to Mn^{3}+-O-Cr^{3+} bonds.

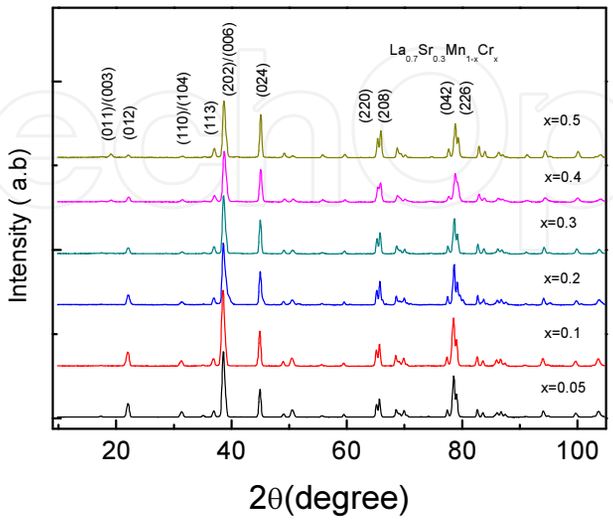

Figure 16. The neutron diffraction patterns of the $La_{0.7}Sr_{0.3}Mn_{1-x}Cr_xO_3$ sample at 10 K.

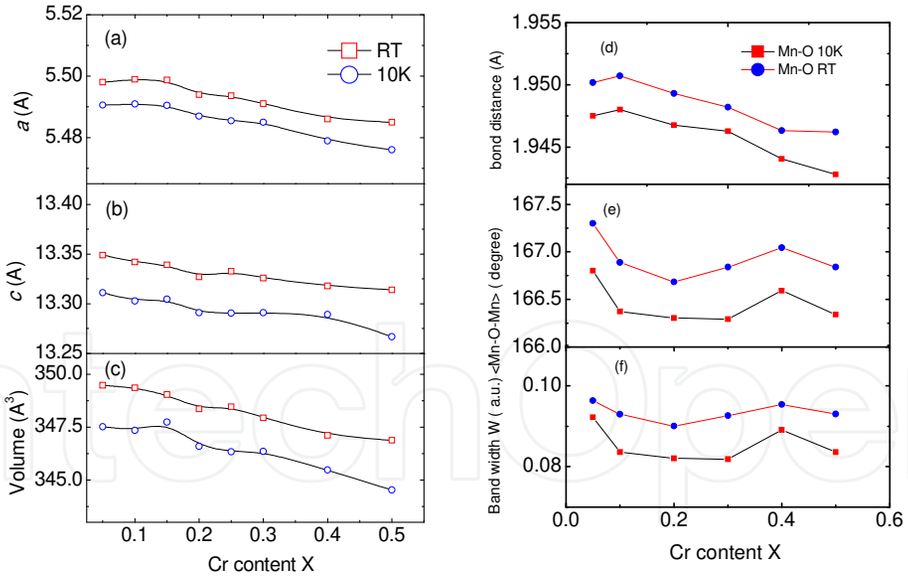

Figure 17. The lattice parameters a, c, unit cell volume, bandwidth *W*, bond length $d_{Mn\text{-}O}$, and bond angle <Mn-O-Mn> for $La_{0.7}Sr_{0.3}Mn_{1-x}Cr_xO_3$ at RT and 10 K.

At low temperature with small x, the net ferromagnetic behavior of the system is due to the large quantities of Mn^{3+}-O-Mn^{4+} ferromagnetic double exchanges taking place while the system is being driven towards a layered ferromagnetic structure by the antiferromagnetic Cr^{3+}-O-Mn^{4+} superexchanges. In the intermediate region (0.2<x<0.4) charge ordering creates a layered

http://dx.doi.org/10.5772/61770

structure and the antiferromagnetic Cr^{3+}-O-Mn^{4+} superexchange continues to drive the system towards an antiferromagnetic state. As x>0.4, the antiferromagnetic Cr^{3+}-O-Cr^{3+} and Cr^{3+}-O-Mn^{4+} superexchange mechanisms become dominate, with charge order persisting, producing a ferrimagnetic structure in lieu of an antiferromagnetic one.

Figure 17 displays the refined lattice parameters, unit cell volume, bond length $d_{Mn\text{-}O}$, bond angle <Mn-O-Mn>, and band width *W* of $La_{0.7}Sr_{0.3}Mn_{1-x}Cr_xO_3$ samples at RT and 10 K. It can be seen that that the lattice parameters, cell volume and bond distance slightly decrease with increasing the Cr content x, which originates from the fact that the radius of Cr ions (0.615 Å for Cr^{3+}) is little bit smaller than that of Mn ions (0.65 Å for Mn^{3+}). The Mn-O-Mn bond angle decreases to a minimum for x=0.2 and then increases to a maximum for x=0.4. A similar trend can be observed for the band width *W*. This is consistent with the fact that a charge ordering creates a layered structure and the antiferromagnetic Cr^{3+}-O-Mn^{4+} superexchange continues to drive the system towards an antiferromagnetic state.

4. Conclusion

The B-site substituted LSMOs can be divided into following two groups, (1) those made with the replacement of Mn by other 3d transition metal ions and (2) those made with the replacement of Mn by non-magnetic, closed shell, metal ions such as Ti, Zr. The ionic radii of the substituted elements, the Mn-O-Mn bond angles, the Mn-O bond length, the calculated bandwidths W, and the corresponding T_C's are given in Table I. It should be pointed out that neutron diffraction scattering lengths of the 3d elements are sufficiently different, and uniquely, the scattering length of Mn is negative. This allows relatively small amounts of other elements substituted into the manganites to be accurately located in the unit cell structure by employing neutron diffraction.

Substituted atom	**Electronic configuration**	**Ionic radius (Å)**	Mn-O bond length (Å)	**Mn-O-Mn bond angle(degree)**	T_C (K) (x=0.1)
Ti^{4+}	[Ar]	0.605	1.9621	165.142	231
Zr^{4+}	[Kr]	0.72	1.9566	166.031	318
Zn^{2+}	[Ar]	0.74	1.9538	166.41	340
Cu^{2+}/Cu^{3+}	[Ar]$3d^9/3d^8$	0.73/0.54	1.9507	166.733	300
Fe^{3+}/Fe^{4+}	[Ar]$3d^5/3d^4$	0.645/0.585	1.9568	166.179	310
Cr^{3+}/Cr^{4+}	[Ar]$3d^3/3d^2$	0.615/0.55	1.9507	166.896	327
$Co^{3}+/Co^{4+}$	[Ar]$3d^6/3d^5$	0.61/0.53	1.9515	166.591	324
Ni^{2+}/Ni^{3+}	[Ar]$3d^8/3d^7$	0.69/0.6	1.9506	166.986	289
Mn^{3+}/Mn^{4+}	[Ar]$3d^4/3d^3$	0.64/0.53	1.9451	166.03	370

Table 1. The electronic configuration, ionic radii, Mn-O bond length and Mn-O-Mn bond angle at room temperature, and T_C for $La_{0.7}Sr_{0.3}Mn_{1-x}M_xO_3$ (x=0.1, M = Ti, Zr, Zn, Cr, Fe, Co, Ni, and Cu).

4.1. Substitution the Mn-site by 3d-transition metals (TM); Cr, Fe, Co, Ni, Cu

For the TM-substituted LSMOs, they show the same crystal structure with space group $R\bar{3}c$. There are small changes in the lattice parameters, and almost the same valence-band structures near the Fermi level are observed. A decrease in T_C is observed for all elements and a metal to insulator (MIT) transition occurs with increasing substitution content around x=0.2. The decrease in T_C of the parent LSMO with substitution by other 3d transition metals is strongly related to the following two factors; (i) the magnetic moments of the substituting ions and (ii) the ionic radius mismatch between the substituting ion and Mn ions. For the TM-substituted LSMO, the degree of reduction in T_C and saturation magnetization is related to the valence states of the substituting ions and the ionic size mismatch. The highest T_C is obtained from the Cr- and Co-substituted LSMO. This is mainly due to the large magnetic moments of Cr and Co ions and also to the formation of the additional DE interactions between Cr and Mn (or between Co ions). Of the six transition metal-substituted systems, the Cr-based system presented some of the most interesting magnetic properties, followed by the Ni-based system and, finally, the Cu-based system. All systems exhibit layered magnetic behavior, a reduction in ferromagnetism with increasing transition metal content, complex magnetic interactions well below T_C, and a metal to insulator transition around x~0.2 (a value also near the percolation threshold described in many works of around x~0.16). Our data for the Ni [7, 9] and Cr [8] systems strongly suggest the onset of charge ordering occurs coincident with the metal to insulator transition, and not only at specific nodal quantities. We suggest this type of ordering is highly likely in the remaining transition metal-substituted systems, but that additional analysis with neutron data is needed.

4.2. Substitution of the Mn-site by closed shell ions: Ti, Zr or Zn

There are several advantages in using closed shell ions to investigate metal substituted-LSMOs. First, the closed shell ions normally do not affect the magnetic interactions between the Mn ions due to their having no magnetic moment. Second, they have inert gas configurations, and therefore do not contribute to the electron charge density. But there still remains the possibility of secondary effects such as a disturbance of the magnetic ordering and a redistribution of electron charge density by a large ionic size mismatch at the B-site, as with, e.g. Zr^{4+}. In general a decrease in T_C and M_S with increasing substitution is observed for the closed shell ion-substituted LSMOs. This is attributed to the dilution of the magnetic ions and the weakening of the ferromagnetic DE interaction between them. Substitution with Ti is selective because Ti^{4+} substitutes for Mn^{4+}. It would be expected as well that Zr^{4+} or Zn^{2+} would substitute for Mn^{4+}. However the severe ionic size mismatch of $Zr^{4+}$and Zn^{2+} may not allow the substitution of Mn^{4+} by Zr^{4+} or Zn^{2+}. Therefore mixed-valent Mn ions in LSMO are selectively diluted by partial substitution of Mn by these ions. LSMO has the highest T_C when the ratio of Mn^{3+}/Mn^{4+} has an optimal value of 7/3. Upon substitution of the Mn ions with closed shell ions, the ratio of Mn^{3+}/Mn^{4+} deviates from the optimal value of the parent compound. For Ti and Zr substitutions, the Mn^{3+}/Mn^{4+} ratio increases with increasing Ti and Zr content. It should be noted that Zn^{2+} replaces Mn^{3+} which has a larger magnetic moment than Mn^{4+}, and the difference of the magnetic moments in the Mn-sites of the Zn-substituted LSMO and Ti- or Zr-

http://dx.doi.org/10.5772/61770

substituted LSMO is only $0.1\mu_B$ per Mn-site. In this case, the competition between DE and SE interactions is a more important control factor for predicting T_C and M_S. Therefore, substitution onto the Mn-site with Zn^{2+} produces more DE couplings and less SE couplings. In turn one would expect the Zn-substituted LSMO to have a larger M_S and a higher T_C than with Ti or Zr substitution, which produces less DE couplings and more SE couplings.

Acknowledgements

This work was supported by the National Natural Science Foundation of China (Grant Nos 51371009, 50971003 and 51171001), the National Basic Research Program of China (No 2010CB833104, MOST of China), the National High Technology Research and Development Program of China (No 2011AA03A403).

Author details

J.B. Yang[1,2*], M.S. Kim[3], T. F. Creel[3], H. Zhao[1], X.G. Chen[1], W.B. Yelon[3] and W.J. James[3]

*Address all correspondence to: jbyang@pku.edu.cn

1 State Key Laboratory for Mesoscopic Physics, School of Physics, Peking University, Beijing, P. R. China

2 Collaborative Innovation Center of Quantum Matter, Beijing, P. R. China

3 Materials Research Center, Missouri University of Science and Technology, USA

References

[1] Ahn, K. H. ; Wu, X. W. ; Liu, K. ; & Chien, C. L. (1996). Magnetic properties and colossal magnetoresistance of La(Ca)MnO_3 materials doped with Fe, Phys. Rev. B 54, 15299.

[2] Ahn, K. H. ; Wu, X. W. ; Liu, K. ; & Chien, C. L. (1997). Effects of Fe doping in the colossal magnetoresistive $La_{1-x}Ca_xMnO_3$, J. Appl. Phys., 81, 5505.

[3] Alexandrov, A. S. ; & Bratkovsky, A. M. (1999). Carrier Density Collapse and Colossal Magnetoresistance in Doped Manganites, Phys. Rev. Letter., 82, 141.

[4] Anderson, P. W.; & Hasegawa, H. (1955). Considerations on Double Exchange, Phys. Rev., 100, 675.

[5] Blasco, J. ; Garcia, J. ; de Teresa, J. M. ; Ibarra,M. R. ; Perez, J. ; Algarabel, P. A. ; Marquina, C. ; & Ritter, C. (1997). Structural, magnetic, and transport properties of the giant magnetoresistive perovskites $La_{2/3}Ca_{1/3}Mn_{1-x}Al_xO_{3-\delta}$ Phys. Rev. B, 8905.

[6] Cao, D. ; Bridges, F. ; Anderson, M. ; Ramirez, A. P. ; Olapinski, M. ; Subramanian, M. A. ; Booth, C. H. ; and Kwei, G. H. (2001). Local distortions in $La_{0.7}Ca_{0.3}Mn_{1-b}A_bO_3$ (A=Ti and Ga) colossal magnetoresistance samples: Correlations with magnetization and evidence for cluster formation, Phys. Rev. B. , 64, 184409.

[7] Creel, Thomas F.; Yang, Jinbo; Kahveci, Mehmet; Malik, Satish K.; Quezado, S.; Pringle, O.A.; Yelon, William B.; & James, William J. (2013a). Structural and magnetic properties of $La_{0.7}Sr_{0.3}Mn_{1-x}Ni_xO_3$ (x<=0.4), Journal of Applied Physics, 114(1), 013911.

[8] Creel, Thomas F.; Jinbo Yang, Kahveci, Mehmet; Lamsal, Jagat; Malik, S. K.; Quezado, Sylvio; Pringle, Oran A.; Yelon, William B.; & James, William J. (2010). Structural and Magnetic Properties of $La_{0.7}Sr_{0.3}Mn_{1-x}Cr_xO_3$ (x<= 0.5), IEEE Transactions on Magnetics 46(6), 1832-1835.

[9] Creel, Thomas F. (2013b). Structural and magnetic properties of Ni and Cr substituted $La_{0.7}Sr_{0.3}MnO_3$, Doctoral Dissertations. Paper 2031.

[10] Dai, P. ; et al., (1996). Experimental Evidence for the Dynamic Jahn-Teller Effect in $La_{0.65}Ca_{0.35}MnO_3$, Phys. Rev. B 54, R3694.

[11] De, Gennes P. G. (1960). Effects of Double Exchange in Magnetic Crystals, Phys. Rev., 118, 141.

[12] Dessau, D. S. ; Saitoh, T.; Park, C. H.; Shen, Z. X. ; Villella, P. ; Hamad,a N. ; Moritomo, Y. ; and Tokura, Y. (1998). k-dependent electronic structure, a large "ghost" fermi surface, and a pseudogap in a layered mangnetoresistive oxide, Phys. Rev. Lett., 81, 192.

[13] Dho, J. ; Kim, W. S.; & Hur, N. H. (2002). Reentrant Spin Glass Behavior in Cr-Doped Perovskite Manganite, Phys. Rev. Lett. 89, 027202.

[14] Geck, J.; et al., (2001). Evidence for canted antiferromagnetism in lightly doped $La_{1-x}Sr_xMnO_3$, Phys. Rev. B 64, 144430.

[15] Hwang, H. Y.; Cheong, S-W.; Radaelli, P. G.; Marezio, M.; & Batlogg, B. (1995). Lattice Effects on the Magnetoresistance in Doped $LaMnO_3$, Phys. Rev. Lett. 75, 914.

[16] Harrison, W. A. (1980) The electronic structure and properties of solids (Freeman, San Francisco, 1980).

[17] Imada, M. ; Fujimori, A.; & Tokura, Y. (1998). Metal-insulator transitions, Rev. Mod. Phys. 70, 1039.

[18] Joly, V. L. J. ; Joy, P. A. ; Date, S. K. ; & Gopinath, C. S. (2002). Two ferromagnetic phases with different spin states of Mn and Ni in $LaMn_{0.5}Ni_{0.5}O_3$, Phys. Rev. B 65, 184416.

[19] Ju, H. L. ; Sohn, H. C. ; & Krishnan, K. M. (1997). Evidence for O-2p hole-driven conductivity in $La_{1-x}Sr_xMnO3$ ($0 \leq x \leq 0.7$) and $La_{1-x}Sr_xMnOz$ thin films, Phys. Rev. Lett., 74, 3230 (1997).

[20] Kubo, K.; & Ohata, N. (1972). A Quantum Theory of Double Exchange, J. Phys. Soc. Japan ,33, 21-32.

[21] Kim, K. H. ; Jung, J. H. ; & Noh, T. W. (1998). Polaron Absorption in a Perovskite Manganite $La_{0.7}Ca_{0.3}MnO_3$, Phys. Rev. Lett., 81, 1517.

[22] Kim, M. S. ; Yang, J. B. ; Cai, Q.; Zhou, X. D.; James, W. J.; Yelon, W. B.; Parris, P. E.; Buddhikot, D.; & Malik, S. K. (2005a). Structure, magnetic and transport properties of Ti-substituted $La_{0.7}Sr_{0.3}MnO_3$, Phys. Rev. B. 71, 14433.

[23] Kim, M. S.; Yang, J. B.; Cai, Q.; James, W. J.; Yelon, W. B.; Parri,,P. E.;& Malik, S. K. (2007). Structural, magnetic, and transport properties of Zr-substituted $La_{0.7}Sr_{0.3}Mn_{1-x}O_3$, J. Appl. Phys. 102, 013531.

[24] Kim, M. S.; Yang, J. B.; Cai, Q.; Zhou, X.D.; James, W. J.; Yelon, W. B.; Parri, P. E.; & Malik, S. K. (2005b). The effect of Cu-doping on the magnetic and transport properties of $La_{0.7}Sr_{0.3}MnO_3$, J. Appl. Phys. 97, 10H714.

[25] Kim, M.S. ; Yang, J.B. ; Cai, Q. ; Zhou, X.D.; James ,W.J.; Yelon,W.B.; & Parris, P.E., (2008). Electronic structure of $La_{0.7}S_{0.3}Mn_{1-x}Cu_xO_3$, J. Phys. C: Condensed Matter 20, 255228/1.

[26] Kimura, T. ; Tomioka, Y. ; Kumai, R. ; Okimoto, Y. ; & Tokura, Y. (1999). Diffuse Phase Transition and Phase Separation in Cr-Doped $Nd_{1/2}Ca_{1/2}MnO_3$: A Relaxor Ferromagnet, Phys. Rev. Lett. 83, 3940

[27] Klingeler, R. ; Geck J. ; Gross, Pinsard-Gaudart L. ; Revcolevschi, A. ; Uhlenbruck S.; & Büchner, B. (2002). Magnetism and the charge order transition in lightly doped $La_{1-x}Sr_xMnO_3$, Phys. Rev. B 65, 174404.

[28] Liu, X. ; Xu, X. ; & Zhang, Y. (2000). Effect of Ti dopant on the carrier density collapse in colossal magnetoresistance material $La_{0.7}Ca_{0.3}Mn_{1-y}Ti_yO_3$ Phys. Rev. B 62, 15112.

[29] Medarde, M. ; Mesot, J. ; Lacorre, P. ; Rosenkranz, S. ; Fischer, P. ; & Gobrecht, K. (1995). High-pressure neutron-diffraction study of the metallization process in PrNiO3, Phys. Rev. B 52, 9248.

[30] Millis, A. J. ; Littlewood, P. B. ; & Shraiman, B. I. (1995). Double Exchange Alone Does Not Explain the Resistivity of $La_{1-x}Sr_xMnO_3$, Phys. Rev. Lett., 74, 5144.

[31] Millis, A. J. ; Shraiman, B. I.; & Mueller, R. (1996). Dynamic Jahn-Teller Effect and Colossal Magnetoresistance in $La_{1-x}Sr_xMnO_3$, Phys. Rev. Lett., 77,175.

[32] Neumeier, J. J. ; Andres, K. ; and McClellan, K. J. (1999). Thermal expansion of single-crystalline $La_{0.83}Sr_{0.17}MnO_3$: The importance of temperature-induced strain for the electrical resistivity, Phys. Rev. B , 59, 1701.

[33] Okada, K. ; & Yamada, S. (2012). Anisotropic magnetic properties of $P_{1-x}Ca_xMnO_3$, Phys. Rev. B 86, 064430

[34] Ogale, S. B. ; Shreekala, R.; Bathe, R. ; Date, S. K. ; Patil, S. I. ; Hannoyer, B. ; Petit, F. ; & Marest, G. (1998). Transport properties, magnetic ordering, and hyperfine interactions in Fe-doped $La_{0.75}Ca_{0.25}MnO_3$: Localization-delocalization transition, Phys. Rev. B 57, 7841.

[35] Radaelli, P. G. ; Iannone, G., Marezio, M. ; Hwang, H. Y. ; Cheong, S-W.; Jorgensen, J. D. ; & Argyriou, D. N. (1997). Structural effects on the magnetic and transport properties of perovskite A_{1-x} A'_x MnO_3 (x=0.25, 0.30), Phys. Rev. B 56, 8265 (1997).

[36] Raveau, B. ; Maignan, A. ; & Martin, C. (1997). Insulator–Metal Transition Induced by Cr and Co Doping in $Pr_{0.5}Ca_{0.5}MnO_3$, Journal of Solid State Chemistry, 130, 162–166

[37] Salamon, Myron B. ; & Jaime, M. (2001). The physics of manganites: Structure and transport, Rev. Mod. Phys. 73, 583.

[38] Shannon, R. D. (1976). Revised effective ionic radii and systematic studies of interatomic distances in halides and chalcogenides, Acta Crystallogr. Sect. A: Cryst. Phys., Diffr., Theor. Gen. Crystallogr., 751.

[39] Tokura, Y.; Kuwahara, H.; Moritomo, Y.; Tomioka, Y.; & Asamitsu, A. (1996). Competing Instabilities and Metastable States in $(Nd,Sm)_{1/2}Sr_{1/2}MnO_3$, Phys. Rev. Lett. 76, 3184.

[40] Zener C. (1951). Interaction between the d -Shells in the Transition Metals. II. Ferromagnetic Compounds of Manganese with Perovskite Structure, Phys. Rev., 82, 403.

[41] Zhao, G. M. ; Smolyaninova, V. ; Prellie,r W. ; & Keller, H. (2000). Electrical transport in the ferromagnetic state of manganites: Small-polaron metallic condition at low temperatures, Phys. Rev. Lett. 84, 6086.